

# On synchronous supereruptions

A. Cisneros de León<sup>1\*†</sup>, T. Mittal<sup>2\*†</sup>, S.L. de Silva<sup>3</sup>, S. Self<sup>4</sup>, A.K. Schmitt<sup>1</sup>, S. Kutterolf<sup>5</sup>

<sup>1</sup>Institute of Earth Sciences, Heidelberg University; Heidelberg, Germany.

<sup>2</sup>Department of Earth, Atmosphere and Planetary Sciences, Massachusetts Institute of Technology; Cambridge, USA.

<sup>3</sup>College of Earth, Ocean, and Atmospheric Sciences, Oregon State University; Corvallis, USA.

<sup>4</sup>Earth and Planetary Science Department, University of California; Berkeley, USA.

<sup>5</sup>GEOMAR Helmholtz Centre for Ocean Research; Kiel, Germany.

\*Corresponding author. Email: cisneros.deleon@outlook.de

†These authors contributed equally to this work.

## Abstract

Two recent supereruptions (magnitude (M) scale  $\geq 8$ ), the Young Toba Tuff (YTT), Sumatra, and the Los Chocoyos (LCY), Guatemala, are found to be statistically synchronous at ca. 74 ka and near antipodal. Such planetwide synchronicity of supereruptions is shown to be statistically non-random implying a causal link. We propose that the seismic energy release from the YTT supereruption may have initiated eruption from the contemporaneous “perched” LCY magma system. This near-equatorial supereruption “double-whammy” may be the more compelling source of the significant environmental impacts often attributed to a singular YTT eruption.

**Keywords:** Young Toba Tuff, Los Chocoyos, Climate Change

## Introduction

Catastrophic caldera-forming supereruptions are next to the impact of kilometer-sized bolides, the most intense events affecting the Earth system. These low-frequency but high-intensity volcanic “Black Swans” are capable of explosively ejecting  $\geq 1000 \text{ km}^3$  of high-silica tephra at geologically instantaneous timescales (magnitude (M) scale  $\geq 8$ ) (Pyle, 2015). The recorded and expected impacts of such supereruptions range from local to global in scale: complete devastation up to hundreds of kilometers away from the eruptive vent by ground-hugging hot

30 and turbulent pyroclastic density currents (Roche et al., 2016) and regional-scale economic,  
 31 social, and eco-system disruption by tephra fall (Miller and Wark, 2008), that may extend to  
 32 the global scale over several years to decades through the release of significant amounts of  
 33 climate-forcing gases such as sulfur, chlorine, and bromine (Brenna et al., 2020; Brenna et al.,  
 34 2021; Self, 2015).

35 In the last 2 Myr, at least 13 supereruptions have occurred globally (Crowweller et al., 2012)  
 36 with an estimated recurrence interval of *ca.* 150 kyr, a timescale shorter than the frequency of  
 37 meteorite impacts (*ca.* 0.6-3 Myr)(Bland, 2005) large enough to potentially have similar  
 38 environmental consequences (Rampino, 2002). If the eruption record of only the last *ca.* 100  
 39 kyr is considered, the recurrence interval further decreases to *ca.* 17 kyr (Rougier et al., 2018).  
 40 Given the likelihood that established eruption databases are incomplete (Crowweller et al., 2012)  
 41 these rates could be considered maxima and a temporal coincidence of supereruptions is not *a*  
 42 *priori* unlikely. Synchronous, paired, or grouped, large (M7 to M8) eruptions have been  
 43 proposed within various volcanic regions (e.g., de Silva et al., 2006; Gravley et al., 2007), but  
 44 synchronicity of eruptions  $\geq$ M8 on a global scale is hitherto unknown. The discovery of two  
 45 apparently synchronous recent supereruptions, the *ca.* 74 ka Young Toba Tuff (YTT), Sumatra,  
 46 and Los Chocoyos (LCY), Guatemala, has implications for the global record of supereruptions  
 47 and warrants an evaluation of the randomness of paired eruptions at the colossal scale.

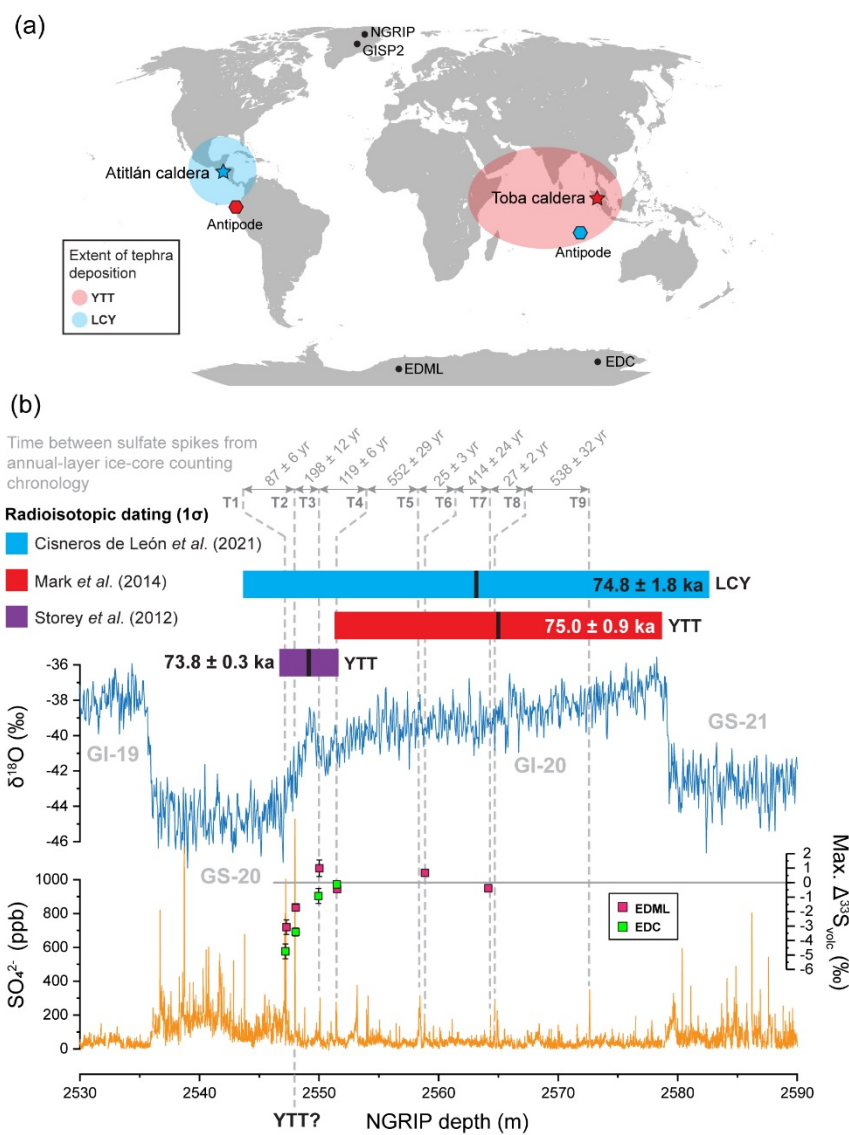
#### 48 **Constraints on the timing of YTT and LCY supereruption**

49 Until recently, only three supereruptions had been recognized in the last *ca.* 100 kyr (Crowweller  
 50 et al., 2012). Among these the YTT event stands out as the largest supereruption in the  
 51 Quaternary period, discharging more than 8,600 km<sup>3</sup> tephra (M9.1; Costa et al., 2014) with  
 52 fallout deposition over an area of ~40 million km<sup>2</sup> (Fig. 1a). The potential release of significant  
 53 amounts of sulfur gases during this eruption has been putatively linked to a major global  
 54 climatic downturn reflected in the oxygen isotope record of the Greenland ice cores between

55 Greenland interstadial 20 and stadial 20 that may have challenged the survival of modern  
 56 humans (Ambrose, 1998; Rampino and Self, 1992) (Fig. 1b). This hypothesis has been debated  
 57 due to uncertainties about total sulfur released during the eruption (Oppenheimer, 2002; Robock  
 58 et al., 2009), the relatively low-precision of existing radioisotopic ages, and YTT volcanic glass  
 59 shards remaining elusive in ice core records (Abbott et al., 2012; Svensson et al., 2013).  
 60 However, recent work is tilting the evidence towards a significant environmental impact  
 61 associated with a solar ultraviolet radiation catastrophe from extreme ozone depletion after the  
 62 YTT supereruption (Osipov et al., 2021).

63 Because glass shards of the YTT have not been identified in northern and southern hemisphere  
 64 ice core archives, the exact  $\text{SO}_4^{2-}$  spike related to YTT remains ambiguous (Oppenheimer,  
 65 2002; Robock et al., 2009; Williams, 2012). Nevertheless, prominent sulfate anomalies  
 66 occurring in both north and south pole ice-core records have been correlated with YTT (e.g.,  
 67 T2 sulfate spike, Fig. 1b and Fig. S1). However, eight other significant volcanic-derived sulfate  
 68 anomalies from unknown sources (T1-T9; Fig. 1b and Fig. S1) occur within the uncertainty of  
 69 the currently accepted radioisotopically determined eruption ages for YTT between  $73.9 \pm 0.3$   
 70 ka BP ( $1\sigma$ ;  $^{40}\text{Ar}/^{39}\text{Ar}$  in sanidine)(Storey et al., 2012) and  $75.0 \pm 0.9$  ka BP ( $1\sigma$ ;  $^{40}\text{Ar}/^{39}\text{Ar}$  in  
 71 biotite)(Mark et al., 2014) and also indicate large, tropical eruptions (Svensson et al., 2013).

72 We draw attention to recent work that connotes that the LCY supereruption from the Atilán  
 73 caldera in Guatemala, the most recent one from a volcano in the western hemisphere (Cisneros  
 74 de León et al., 2021), is a potential source for one of these significant sulfate spikes. The age of  
 75 the LCY was initially estimated from  $\delta^{18}\text{O}$  stratigraphy at  $84 \pm 5$  ka BP (Drexler et al., 1980)  
 76 and remained radioisotopically untested for several decades. Recent dating applying (U-Th)/He  
 77 zircon double-dating has produced a radioisotopic age for LCY of  $74.8 \pm 1.8$  ka BP ( $1\sigma$ )  
 78 (Cisneros de León et al., 2021).



79  
80  
81  
82  
83  
84  
85  
86  
87  
88  
89

**Figure 1.** Spatial and geochronological information for YTT and LCY projected over climate and volcanic proxy signals from the northern and southern hemisphere ice core records. a) Map showing the location of Toba (Sumatra) and Atitlán calderas (Guatemala) as well as their respective antipodes (hexagons) along with their approximate tephra distribution. b) Synchronization of YTT and LCY radioisotopic ages and their 1 $\sigma$  uncertainty with the NGRIP oxygen isotope and sulfate concentration records around the Greenland Interstadial 20 (GI-20) and the Greenland Stadial (GS-20) as well as the sulfur isotopic compositions from the EPICA Dronning Maud Land (EDML, Antarctica), and EPICA dome C (EDC, Antarctica) ice core records (Crick et al., 2021). Dashed gray lines indicate the sulfate candidate anomalies for the

90 YTT supereruption in the NGRIP but also present in the Antarctic ice cores (Fig. S1). The  
91 relative timespan between sulfate anomalies is derived from ice-core annual counting layers  
92 from (Svensson et al., 2013). Sulfate anomalies between YTT candidates have been discarded  
93 as volcanic-derived signals by (Svensson et al., 2013), based on the lack of anomalies in other  
94 volcanic eruption proxies in the ice cores like electrical conductivity.

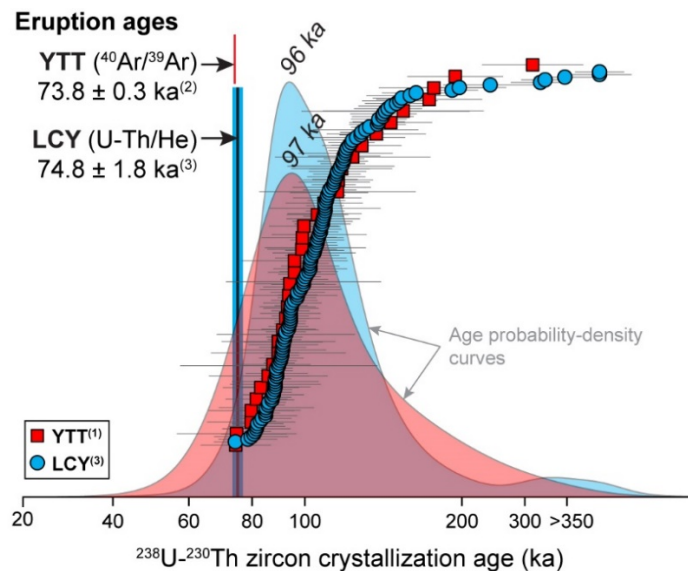
95  
96 The new LCY age is strikingly close to that of YTT (overlapping within  $1\sigma$  error), implying  
97 that in combination both eruptions would potentially have more impact on global climate than  
98 each eruption on its own (e.g., Toohey et al., 2016). Additionally, the close age concordance is  
99 intriguing from the perspective of teleconnections and causative linkages. Both supereruptions  
100 likely deposited relatively high amounts of sulfate on the ice sheets of the northern and southern  
101 hemispheres because of estimated high sulfur loads and tropical vent location (LCY =  $523 \pm 95$   
102 Mt (Brenna et al., 2020); YTT = 1,700–3,500 Mt (Costa et al., 2014)); though significant  
103 uncertainties on the validity of these estimations exists.

#### 104 **Timespan between YTT and LCY**

105 Assuming that the YTT and LCY eruptions are represented by two of the nine sulfate spike  
106 candidates within the YTT eruption window, a relative time difference between the two  
107 supereruptions can be estimated by counting the ice-deposition annual layers (Svensson et al.,  
108 2013) (Fig. 1b). The estimated time window ranges from a maximum of *ca.* 2,000 yr (T1 to T9  
109 spikes) and a minimum of *ca.* 25 yr (T5 to T6 spikes). We note that sulfate spikes (T1–T4)  
110 show large-magnitude sulfur mass-independent fractionation (S-MIF) isotopic signatures (Fig.  
111 1b)(Crick et al., 2021), which are indicative for large eruptions from tropical locations whose  
112 plumes reached altitudes at or above the ozone layer in the stratosphere. If only the spikes  
113 associated with S-MIF are considered the potential maximum and minimum timespan between  
114 YTT and LCY could be further constrained to *ca.* 400 and 87 yr, respectively; orders of  
115 magnitude shorter than the estimated recurrence interval of supereruptions.

116 This close temporal correspondence between YTT and LCY (87–400 yr) is extraordinary given  
 117 that individual supereruptions are extremely rare events in nature. If synchronous  
 118 supereruptions are indeed anomalous events, the temporal proximity of YTT and LCY raises  
 119 the question of whether there is a causal relationship between these two geologically concurrent  
 120 events and if both could have resulted from a third underlying process? The location of Atitlán  
 121 caldera being nearly antipodal to that of Toba caldera is also highly intriguing (Fig. 1a, ~2,200  
 122 km between the Atitlán caldera and the antipodal location of the Toba caldera), as is the almost  
 123 identical zircon crystallization record from both magmatic systems (Fig. 2).

124

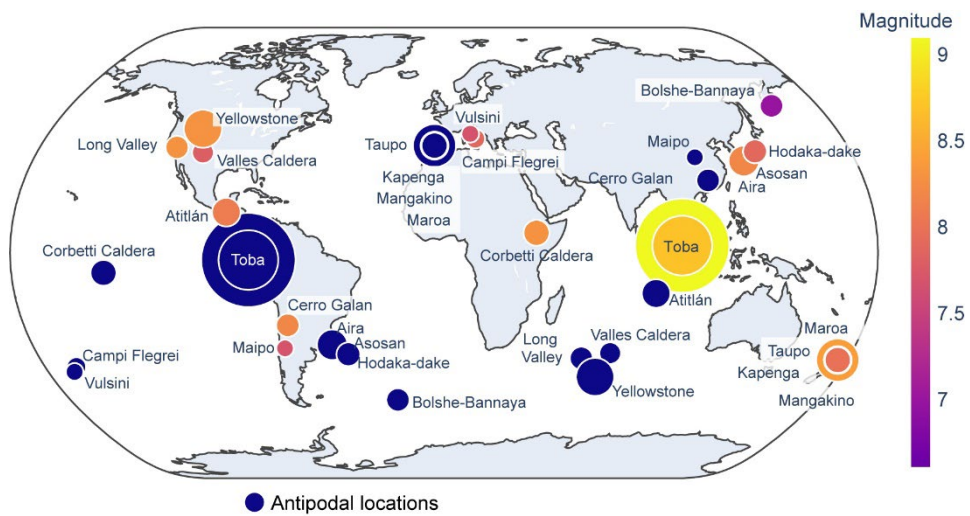


125

126 **Fig. 2.** Ranked order plot and probability-density curves for YTT and LCY zircon rim  
 127 crystallization ages. Vertical bars represent radioisotopic ages for YTT and LCY eruptions,  
 128 with colored-bar thicknesses representing corresponding  $1\sigma$  uncertainty. Data from <sup>1</sup>(Mucek et  
 129 al., 2017), <sup>2</sup>(Storey et al., 2012), and <sup>3</sup>(Cisneros de León et al., 2021).

130 **Supereruption clustering and statistical analysis**

131 Although synchronous large eruptions have been suggested before for the Altiplano Puna  
 132 Volcanic Complex of the Andes and the Taupo Volcanic Zone of New Zealand (de Silva et al.,  
 133 2006; Gravley et al., 2007), these are from coeval regional magmatic systems that reasonably  
 134 could be expected to be linked because of their spatial proximity and thermomechanical  
 135 connectivity. At least in the Altiplano Puna Volcanic Complex, any assessment of true  
 136 synchronicity is obscured by the limited resolution of the radioisotopic techniques. Other  
 137 potential examples of synchronicity on a global scale may be represented by the Huckleberry  
 138 Ridge Tuff (HRT) in the USA ( $2.0794 \pm 0.0046$  Ma)(Rivera et al., 2014) and Cerro Galán  
 139 Ignimbrite (CGI) in Chile ( $2.08 \pm 0.02$  Ma)(Kay et al., 2011), but these lack the age precision  
 140 to accurately constrain relative ages on a sub-kyr scale. They also lack the near antipodal  
 141 positioning that stands out as a unique and compelling feature of the YTT-LCY connection



142 (Fig. 3).

143  
 144 **Fig. 3.** Large volcanic eruptions (> 400 km³) from the LaMEVE database over the last 2.1 Myr.  
 145 Eruption magnitudes are represented by the size and color of the symbol. The antipodal location  
 146 for each eruption is shown as blue circles. It is noteworthy that the main potentially antipodal  
 147 relationship between two supervolcano eruptions also close in time is the YTT and LCY  
 148 eruption pair. Note that Toba has sourced two Quaternary supereruptions, with YTT represented  
 149 by the larger circle (id. Taupo).

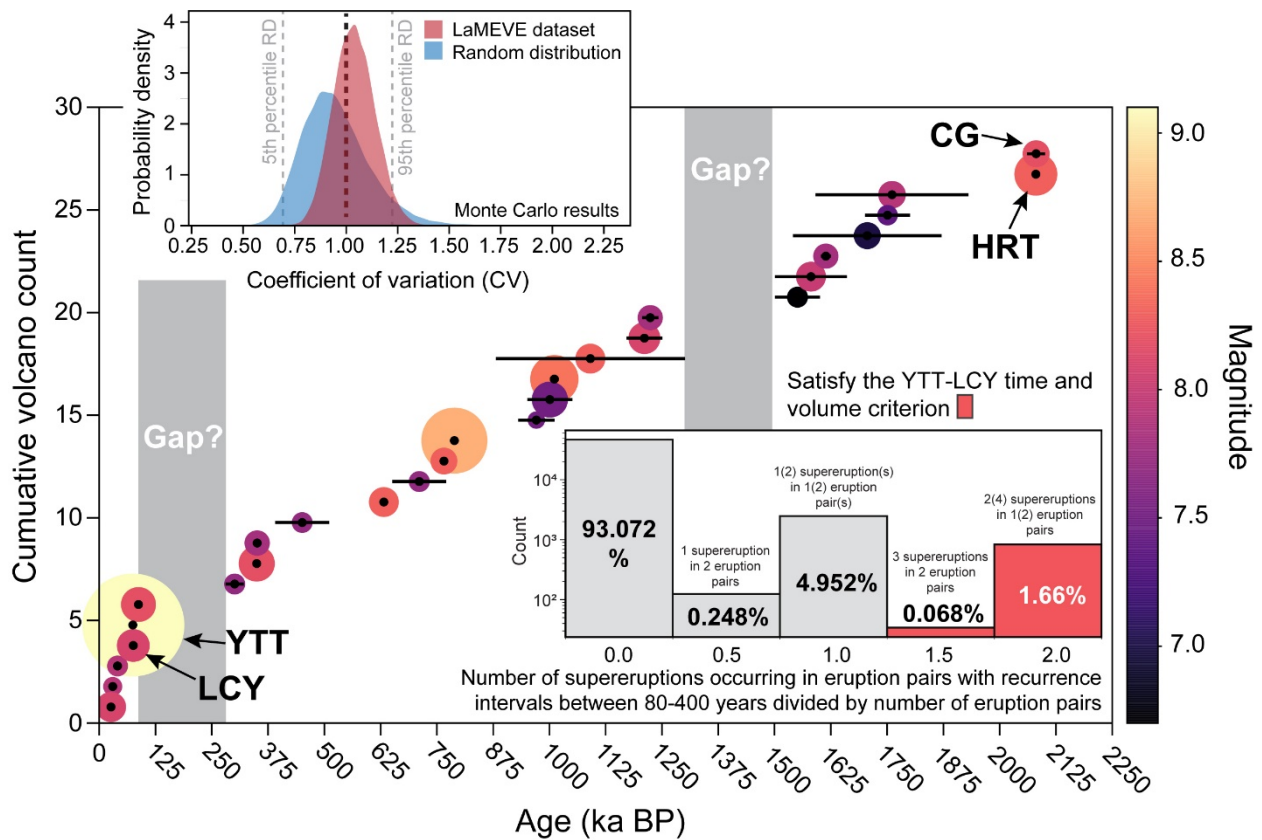


150 We evaluate whether the temporal clustering of large eruptions is purely random using the  
151 timing of  $>400 \text{ km}^3$  bulk volume ( $>M7$ ) Quaternary eruptions (LaMEVE)(Crowweller et al.,  
152 2012) that produced well-preserved deposits in the geological record. A relatively lower bulk  
153 volume than supereruptions was chosen to increase the sample size number ( $n = 28$ ) for  
154 statistical analysis in order to avoid bias in the statistical analysis from having two coeval  
155 supereruptions (LCY and YTT) out of 13 in the past *ca.* 2 Myr ( $\sim 10\%$ ). Additionally, this  
156 threshold ensures that our analysis is comparable to the global eruption frequency analysis for  
157 the largest VEI bin (VEI 7.5 and above) in Papale (2018). To assess any temporal eruption  
158 clustering in the geological record spanning the last *ca.* 2 Myr we calculated the coefficient of  
159 variation value (CV: the ratio of the standard deviation and the mean value for the time between  
160 two successive volcanic eruptions) for the reported eruption record ( $n = 28$ ). Given the potential  
161 statistical bias from a small sampling number ( $n = 28$ ), we used a Monte Carlo simulation (for  
162 details see [Methods](#)) to generate 50,000 different possible synthetic eruption histories after the  
163 reported eruption record and their  $1\sigma$  uncertainties. The resulting median value of the CV for  
164 the reported eruption record distribution is  $\sim 1.035$ , whereas the median value of the mean time  
165 between eruptions is 76.28 kyr (28 eruptions in 2.054 Myr). Using the CV values obtained from  
166 the synthetic sequences of  $n$  equal to that of the reported Quaternary large eruptions ( $n = 28$ ),  
167 we find that our  $>400 \text{ km}^3$  bulk volume LaMEVE distribution lies within the 5–95th percentile  
168 for a random distribution (inset [Fig. 4](#)). Thus, LaMEVE dataset as a whole does not display any  
169 significant non-randomness/clustering at the 95% confidence limit. This conclusion is further  
170 supported by the clear difference in the CV value between the LaMEVE dataset and synthetic  
171 eruption histories with either periodically spaced eruptions or close eruption pairs ( $\sim 5\%$  of the  
172 average time between eruption groups, [Fig. S2](#)). We would note that some of the statistical  
173 properties of the LaMEVE dataset are not fully consistent with a purely random (or Poisson)  
174 eruption history. Specifically, the most likely value for the median temporal gap between  
175 individual eruptions does not closely match the expectations for random eruption histories ([Fig.](#)



176 S3). However, based on our analysis of a variety of synthetic eruption histories (e.g., random,  
 177 periodic, clustered, Fig. S4) and their differences concerning the median parameter, we posit  
 178 that the LaMEVE dataset is likely a mostly random eruptive history with only a few eruption  
 179 pairs (potentially YTT-LCY and HRT-CGI).

180 Finally, we estimate the occurrence of two supereruptions within a time range from 80 to 400  
 181 yr in a random eruptive history. Among 50,000 synthetic histories with random spacing  
 182 between eruptions and volumes sampled from our LaMEVE dataset, we find that only 1.73%  
 183 of the synthetic histories have an eruption pair that matches the YTT-LCY characteristics (Inset  
 184 Fig. 4). The probability is still less than 2% even if we use a homogeneous Poisson process  
 185 (e.g., Papale, 2018) as the model for eruption temporal distribution instead of a random  
 186 distribution. Moreover, even if we assume that the LaMEVE database is only complete for the  
 187 last 100 kyr as suggested by Rougier et al. (2018) (6 eruptions with  $>400 \text{ km}^3$  in last 100 kyr,  
 188 recurrence time of *ca.* 17 kyr), there is still only a 4.2% probability of a YTT-LCY type eruption  
 189 pair (Fig. S6). Thus, the statistical likelihood for two closely spaced supereruptions is small.  
 190 This probability decreases further to only 0.086% when considering only synthetic eruption  
 191 pairs at a comparable spatial distribution to the near antipodal nature of the Toba and Atitlán  
 192 source calderas (Fig. S7) as shown in Fig. 3. Therefore, this spatial relationship between Atitlán  
 193 and Toba is unique amongst any other large eruptions (Fig. 3 with  $>400$  bulk volume eruptions),  
 194 especially the M8 eruptions.



195

196 **Figure 4.** Cumulative number of eruptions (>400 km<sup>3</sup>) through the last *ca.* 2.2 Myr from the  
 197 LaMEVE database. The color and size of the symbols are representing the magnitude of the  
 198 eruptions. Black bars through symbols are 1σ age uncertainties. The upper inset plot shows the  
 199 probability density curves for the coefficient of variation (CV) values from both the reported  
 200 eruption dataset from LaMEVE and that of 50,000 synthetic eruptive histories generated by a  
 201 Monte Carlo algorithm. Values of CV >1 indicate clustering of eruptions and CV <1 periodic  
 202 eruptions. The lower inset histogram shows the number of eruption histories (among 50,000  
 203 synthetic eruptions histories assuming that eruptions are randomly distributed) that contain  
 204 paired eruptions within 80-400 years and at least one supereruption (>1000 km<sup>3</sup>) divided by the  
 205 number of eruption pairs. A paired supereruption with YTT-LCY characteristics would be  
 206 represented by ‘1.5’ or ‘2.0’ (either 1 or 2 eruption pairs) on the x-axis. On the other hand, if  
 207 only one of the two closely spaced eruptions is a supereruption, it would be represented by the  
 208 ‘0.5’ or ‘1’ (either 1 or 2 eruption pairs) bin in the x-axis. The numbers on each histogram show  
 209 the percentage probability of being in that bin based on the synthetic eruptive histories.

## 210 **Physical processes for supereruption initiation**

211 Given the unlikely nature of a randomly synchronous eruption between YTT and LCY, it is  
212 reasonable to consider if there could be a causal relationship between them. The near-antipodal  
213 positions of the Toba caldera in Sumatra and the Atitlán caldera in Guatemala may be key.  
214 Geological effects including extensive crustal fracturing and surface disruption have been  
215 reported in antipodal locations after major meteorite impacts on Mercury and the Moon  
216 resulting from spherical focusing of impact-generated seismic energy (Watts et al., 1991). On  
217 Earth, antipodal effects from meteorite impacts have been potentially associated with the  
218 triggering or enhancing of volcanic activity (Meschede et al., 2011; Richards et al., 2015). Large  
219 magnitude tectonically generated earthquakes have also been associated with antipodal seismic  
220 focusing (O'Malley et al., 2018). Nonetheless, triggering of one supereruption by another from  
221 the seismic moment released, especially lying at the opposite side of the globe, is yet an  
222 undocumented phenomenon and difficult to quantify as instrumental data of the elastic energy  
223 associated with supereruptions are non-existent (Gudmundsson, 2016). This notwithstanding,  
224 we note that an estimate for the total elastic energy released during the Toba supereruption is  
225 in the order of  $10^{19}$  [J] (Gudmundsson, 2016), which is in the same order of magnitude as the  
226 largest instrumentally recorded earthquake, the M9.5 Chile (Valdivia) earthquake. As a  
227 comparison, the energy delivered by a meteorite impact like the Chicxulub event is estimated  
228 in the order of  $\sim 10^{23}$  [J] (Boslough et al., 1996), which translates into seismic energy of  $\sim 10^{18}$ –  
229  $10^{20}$  [J] after conversion into seismic efficiency (Shishkin, 2007). Although the rate of elastic  
230 energy released by the YTT supereruption is likely lower than a M9.5 earthquake or a large  
231 impact (due to much longer eruption duration), the total energy released is similar and may thus  
232 have similar effects on distal magmatic systems. The potential causal relationship between  
233 seismic energy and triggering or initiating of volcanic eruptions remains poorly constrained. It  
234 has been documented for only 0.4% of historical eruptions (Manga and Brodsky, 2006; Sawi

235 and Manga, 2018) though this probability may increase to 10% when considering a 2 yr window  
236 between a leading large earthquake and a subsequent explosive eruption (Sawi and Manga,  
237 2018). Causal effects are further supported by a temporal link between large magnitude  
238 earthquakes and volcanic activity at a global scale that has been proposed for the M9.1 Sumatra  
239 earthquake (Hill-Butler et al., 2020). Seismic activity has also been suggested as a potential  
240 trigger or initiation mechanism of supereruptions from perched magma reservoirs (Davis et al.,  
241 2007; Gregg et al., 2015). The dynamic stresses induced by passing seismic waves have been  
242 linked to the onset of different magmatic processes affecting the host-rock, magma chamber, or  
243 associated hydrothermal system (Seropian et al., 2021). The associated changes in magma  
244 overpressure, hydrothermal fluid pressure, and crustal and magmatic mush permeability can  
245 ultimately lead to an eruption (Davis et al., 2007; Richards et al., 2015; Seropian et al., 2021).

246 Large supereruption-feeding magma systems can remain petrologically buffered and  
247 thermomechanically primed at a critical threshold for extended periods of time (Caricchi and  
248 Blundy, 2015; Gregg et al., 2012). This pre-eruptive tipping point is most likely to be breached  
249 if roof instability can be initiated externally (Gregg et al., 2012). If YTT preceded the LCY and  
250 produced focused seismicity leading to a perturbation in the stress field of the crust below  
251 Atitlán caldera or in the roof of the magma reservoir, an eruption may be initiated and triggered  
252 if the magma was perched at the pre-eruptive tipping point. Long residence in a melt-present  
253 buffered state for both the YTT and LCY supervolcanic magmatic systems is suggested by  
254 protracted zircon crystallization records (Cisneros de León et al., 2021; Mucek et al., 2017;  
255 Reid and Vazquez, 2017). Notably, both LCY and YTT exhibit strikingly similar  
256 thermochemical histories for their corresponding magma reservoirs based on the crystallization  
257 of zircon and its sensitivity to changes in magma chemistry and temperature (Fig. 2). Magma  
258 accumulation timescales inferred from zircon rim crystallization ages of YTT and LCY are on  
259 the order of tens of thousands of years prior to the supereruption, with a remarkably coincident  
260 maximum at *ca.* 96 ka (Fig. 2). This suggests that the main phase of silicic magma

261 differentiation and assembly of a melt-dominated magma body for YTT and LCY likely  
 262 occurred within a similar time window of *ca.* 20 kyr before the eruption. Thus, zircon indicates  
 263 an ongoing evolution of the Atitlán caldera magma reservoir towards a critical state similar to  
 264 that experienced by YTT. In this scenario, we speculate that the passage of large period  
 265 Rayleigh seismic waves through a crystal-mush-dominated reservoir may have affected the  
 266 system's stability ultimately culminating in a supereruption on a decadal-century scale. Some  
 267 potential physical processes include dynamic stresses due to passing seismic waves that induced  
 268 pore pressure variations modifying the permeability structure of the crystalline matrix  
 269 (Holtzman et al., 2003), and/or liquefaction of the crystalline mush (Sumita and Manga, 2008).  
 270 Both of these processes (and similar visco-elastic two-phase instabilities in a magmatic mush)  
 271 would promote new migration pathways for magma to ascend and increase local stresses in the  
 272 magma reservoir ultimately leading to the eruption.

273 One natural expectation from our model is that the YTT event also primed smaller volcanic  
 274 systems. However, given their smaller scale, these smaller eruptions are likely poorly preserved  
 275 in the geologic record and/or remained unstudied. An exception could be the Arce tephra  
 276 erupted from Coatepeque caldera in El Salvador, which produced two large silicic eruptions  
 277 separated only by a couple of hundreds of years ( $\sim 26$  and  $41 \text{ km}^3$ )(Kutterolf et al., 2019) and  
 278 whose age of  $72 \pm 2 \text{ ka}$  (Rose et al., 1999) overlaps that of YTT and LCY.

279 Resolving whether the time-space relationship between YTT and LCY was not purely random  
 280 but influenced by external factors would critically benefit from refining the absolute dating for  
 281 both supereruptions (and other close supereruption pairs), preferentially by applying the same  
 282 geochronological method. This also holds for assessing the climatic consequences of such  
 283 paired supereruptions. The ultimate resolution for the time lapse between YTT and LCY could  
 284 come from the identification of volcanic glass shards from both supereruptions within the ice-  
 285 core layers. We deem such an endeavor promising because glass compositions from YTT and

286 LCY tephra are unambiguously distinct in trace element abundances (Fig. S7). No tangible  
 287 evidence exists for a large extraterrestrial impact contemporaneous to the YTT-LCY eruption  
 288 pair, but because of the low probability of random coincidence of the YTT-LCY supereruptions,  
 289 such a “triple-whammy” scenario cannot be dismissed.

290 **References**

291  
 292 Abbott, P. M., Davies, S. M., Steffensen, J. P., Pearce, N. J., Bigler, M., Johnsen, S. J.,  
 293 Seierstad, I. K., Svensson, A., and Wastegård, S., 2012, A detailed framework of  
 294 Marine Isotope Stages 4 and 5 volcanic events recorded in two Greenland ice-cores:  
 295 Quaternary Science Reviews, v. 36, p. 59-77.  
 296 Ambrose, S. H., 1998, Late Pleistocene human population bottlenecks, volcanic winter, and  
 297 differentiation of modern humans: Journal of Human Evolution, v. 34, no. 6, p. 623-  
 298 651.  
 299 Bland, P. A., 2005, The impact rate on Earth: Philosophical Transactions of the Royal Society  
 300 A: Mathematical, Physical and Engineering Sciences, v. 363, no. 1837, p. 2793-2810.  
 301 Boslough, M., Chael, E., Trucano, T., Crawford, D., and Campbell, D., 1996, Axial focusing  
 302 of impact energy in the Earth's interior: A possible link to flood basalts and hotspots:  
 303 Geological Society of America Special Papers, v. 307, p. 541-550.  
 304 Brenna, H., Kutterolf, S., Mills, M. J., and Krüger, K., 2020, The potential impacts of a  
 305 sulfur- and halogen-rich supereruption such as Los Chocoyos on the atmosphere and  
 306 climate: Atmos. Chem. Phys., v. 20, no. 11, p. 6521-6539.  
 307 Brenna, H., Kutterolf, S., Mills, M. J., Niemeier, U., Timmreck, C., and Krüger, K., 2021,  
 308 Decadal Disruption of the QBO by Tropical Volcanic Supereruptions: Geophysical  
 309 Research Letters, v. 48, no. 5, p. e2020GL089687.  
 310 Brown, S. K., Croweller, H. S., Sparks, R. S. J., Cottrell, E., Deligne, N. I., Guerrero, N. O.,  
 311 Hobbs, L., Kiyosugi, K., Loughlin, S. C., and Siebert, L., 2014, Characterisation of the  
 312 Quaternary eruption record: analysis of the Large Magnitude Explosive Volcanic  
 313 Eruptions (LaMEVE) database: Journal of Applied Volcanology, v. 3, no. 1, p. 1-22.  
 314 Caricchi, L., and Blundy, J., 2015, The temporal evolution of chemical and physical  
 315 properties of magmatic systems: Geological Society, London, Special Publications, v.  
 316 422.  
 317 Cisneros de León, A., Schindlbeck-Belo, J. C., Kutterolf, S., Danišík, M., Schmitt, A. K.,  
 318 Freundt, A., Pérez, W., Harvey, J. C., Wang, K. L., and Lee, H. Y., 2021, A history of  
 319 violence: magma incubation, timing and tephra distribution of the Los Chocoyos  
 320 supereruption (Atitlán Caldera, Guatemala): Journal of Quaternary Science, v. 36, no.  
 321 2, p. 169-179.  
 322 Costa, A., Smith, V. C., Macedonio, G., and Matthews, N. E., 2014, The magnitude and  
 323 impact of the Youngest Toba Tuff super-eruption: Frontiers in Earth Science, v. 2, p.  
 324 16.  
 325 Crick, L., Burke, A., Hutchison, W., Kohno, M., Moore, K. A., Savarino, J., Doyle, E. A.,  
 326 Mahony, S., Kipfstuhl, S., Rae, J. W. B., Steele, R. C. J., Sparks, R. S. J., and Wolff,  
 327 E. W., 2021, New insights into the ~74 ka Toba eruption from sulfur isotopes of polar  
 328 ice cores: Clim. Past Discuss., v. 2021, p. 1-28.  
 329 Croweller, H. S., Arora, B., Brown, S. K., Cottrell, E., Deligne, N. I., Guerrero, N. O.,  
 330 Hobbs, L., Kiyosugi, K., Loughlin, S. C., and Lowndes, J., 2012, Global database on



331 large magnitude explosive volcanic eruptions (LaMEVE): *Journal of Applied*  
 332 *Volcanology*, v. 1, no. 1, p. 1-13.

333 Davis, M., Koenders, M., and Petford, N., 2007, Vibro-agitation of chambered magma:  
 334 *Journal of Volcanology and Geothermal Research*, v. 167, no. 1-4, p. 24-36.

335 de Silva, S., Zandt, G., Trumbull, R., Viramonte, J. G., Salas, G., and Jiménez, N., 2006,  
 336 Large ignimbrite eruptions and volcano-tectonic depressions in the Central Andes: a  
 337 thermomechanical perspective: *Geological Society, London, Special Publications*, v.  
 338 269, no. 1, p. 47-63.

339 Deligne, N. I., Sparks, R. S. J., and Brown, S. K., 2017, Report on potential sampling biases  
 340 in the LaMEVE database of global volcanism: *Journal of Applied Volcanology*, v. 6,  
 341 no. 1, p. 1-5.

342 Drexler, J. W., Rose, W. I., Sparks, R., and Ledbetter, M., 1980, The Los Chocoyos Ash,  
 343 Guatemala: a major stratigraphic marker in Middle America and in three ocean basins:  
 344 *Quaternary Research*, v. 13, no. 3, p. 327-345.

345 Gravley, D., Wilson, C., Leonard, G., and Cole, J., 2007, Double trouble: Paired ignimbrite  
 346 eruptions and collateral subsidence in the Taupo Volcanic Zone, New Zealand:  
 347 *Geological Society of America Bulletin*, v. 119, no. 1-2, p. 18-30.

348 Gregg, P., De Silva, S., Grosfils, E., and Parmigiani, J., 2012, Catastrophic caldera-forming  
 349 eruptions: Thermomechanics and implications for eruption triggering and maximum  
 350 caldera dimensions on Earth: *Journal of Volcanology and Geothermal Research*, v.  
 351 241, p. 1-12.

352 Gregg, P. M., Grosfils, E. B., and de Silva, S. L., 2015, Catastrophic caldera-forming  
 353 eruptions II: The subordinate role of magma buoyancy as an eruption trigger: *Journal*  
 354 *of Volcanology and Geothermal Research*, v. 305, p. 100-113.

355 Gudmundsson, A., 2016, The mechanics of large volcanic eruptions: *Earth-science reviews*, v.  
 356 163, p. 72-93.

357 Guttorp, P., and Thompson, M. L., 1991, Estimating second-order parameters of volcanicity  
 358 from historical data: *Journal of the American Statistical Association*, v. 86, no. 415, p.  
 359 578-583.

360 Hill-Butler, C., Blackett, M., Wright, R., and Trodd, N., 2020, The co-incidence of  
 361 earthquakes and volcanoes: assessing global volcanic radiant flux responses to  
 362 earthquakes in the 21st century: *Journal of Volcanology and Geothermal Research*, v.  
 363 393, p. 106770.

364 Holtzman, B., Groebner, N., Zimmerman, M., Ginsberg, S., and Kohlstedt, D., 2003, Stress-  
 365 driven melt segregation in partially molten rocks: *Geochemistry, Geophysics,*  
 366 *Geosystems*, v. 4, no. 5.

367 Hooker, J., Laubach, S., and Marrett, R., 2018, Microfracture spacing distributions and the  
 368 evolution of fracture patterns in sandstones: *Journal of Structural Geology*, v. 108, p.  
 369 66-79.

370 Kay, S. M., Coira, B., Wörner, G., Kay, R. W., and Singer, B. S., 2011, Geochemical, isotopic  
 371 and single crystal  $^{40}\text{Ar}/^{39}\text{Ar}$  age constraints on the evolution of the Cerro Galán  
 372 ignimbrites: *Bulletin of Volcanology*, v. 73, no. 10, p. 1487-1511.

373 Kutterolf, S., Schindlbeck- Belo, J. C., Rohr, I., Rademacher, M., Cisneros de León, A.,  
 374 Eisele, S., Freundt, A., Hernandez, W., and Wang, K. L., 2019, The Arce Tephra: Two  
 375 subsequent paroxysmal Plinian eruptions from Coatepeque Caldera (El Salvador):  
 376 *Journal of Volcanology and Geothermal Research*, p. 106673.

377 Manga, M., and Brodsky, E., 2006, Seismic triggering of eruptions in the far field: Volcanoes  
 378 and geysers: *Annu. Rev. Earth Planet. Sci.*, v. 34, p. 263-291.

379 Mark, D. F., Petraglia, M., Smith, V. C., Morgan, L. E., Barfod, D. N., Ellis, B. S., Pearce, N.  
 380 J., Pal, J., and Korisettar, R., 2014, A high-precision  $^{40}\text{Ar}/^{39}\text{Ar}$  age for the Young  
 381 Toba Tuff and dating of ultra-distal tephra: Forcing of Quaternary climate and



382 implications for hominin occupation of India: *Quaternary Geochronology*, v. 21, p. 90-  
 383 103.

384 Meschede, M. A., Myhrvold, C. L., and Tromp, J., 2011, Antipodal focusing of seismic waves  
 385 due to large meteorite impacts on Earth: *Geophysical Journal International*, v. 187, no.  
 386 1, p. 529-537.

387 Miller, C. F., and Wark, D. A., 2008, Supervolcanoes and their explosive supereruptions:  
 388 *Elements*, v. 4, no. 1, p. 11-15.

389 Mucek, A. E., Danišik, M., de Silva, S. L., Schmitt, A. K., Pratomo, I., and Coble, M. A.,  
 390 2017, Post-supereruption recovery at Toba Caldera: *Nature Communications*, v. 8, no.  
 391 1, p. 15248.

392 O'Malley, R. T., Mondal, D., Goldfinger, C., and Behrenfeld, M. J., 2018, Evidence of  
 393 systematic triggering at teleseismic distances following large earthquakes: *Scientific*  
 394 *reports*, v. 8, no. 1, p. 1-12.

395 Oppenheimer, C., 2002, Limited global change due to the largest known Quaternary eruption,  
 396 Toba~ 74 kyr BP?: *Quaternary Science Reviews*, v. 21, no. 14-15, p. 1593-1609.

397 Osipov, S., Stenchikov, G., Tsigaridis, K., LeGrande, A. N., Bauer, S. E., Fnais, M., and  
 398 Lelieveld, J., 2021, The Toba supervolcano eruption caused severe tropical  
 399 stratospheric ozone depletion: *Communications Earth & Environment*, v. 2, no. 1, p.  
 400 1-7.

401 Papale, P., 2018, Global time-size distribution of volcanic eruptions on Earth: *Scientific*  
 402 *reports*, v. 8, no. 1, p. 1-11.

403 Pearce, N. J., Westgate, J. A., Gualda, G. A., Gatti, E., and Muhammad, R. F., 2020, Tephra  
 404 glass chemistry provides storage and discharge details of five magma reservoirs which  
 405 fed the 75 ka Youngest Toba Tuff eruption, northern Sumatra: *Journal of Quaternary*  
 406 *Science*, v. 35, no. 1-2, p. 256-271.

407 Pyle, D. M., 2015, Sizes of volcanic eruptions, *The encyclopedia of volcanoes*, Elsevier, p.  
 408 257-264.

409 Rampino, M. R., 2002, Supereruptions as a threat to civilizations on Earth-like planets: *Icarus*,  
 410 v. 156, no. 2, p. 562-569.

411 Rampino, M. R., and Self, S., 1992, Volcanic winter and accelerated glaciation following the  
 412 Toba super-eruption: *Nature*, v. 359, no. 6390, p. 50-52.

413 Reid, M. R., and Vazquez, J. A., 2017, Fitful and protracted magma assembly leading to a  
 414 giant eruption, Youngest Toba Tuff, Indonesia: *Geochemistry, Geophysics,*  
 415 *Geosystems*, v. 18, no. 1, p. 156-177.

416 Richards, M. A., Alvarez, W., Self, S., Karlstrom, L., Renne, P. R., Manga, M., Sprain, C. J.,  
 417 Smit, J., Vanderkluisen, L., and Gibson, S. A., 2015, Triggering of the largest Deccan  
 418 eruptions by the Chicxulub impact: *Bulletin*, v. 127, no. 11-12, p. 1507-1520.

419 Rivera, T. A., Schmitz, M. D., Crowley, J. L., and Storey, M., 2014, Rapid magma evolution  
 420 constrained by zircon petrochronology and  $^{40}\text{Ar}/^{39}\text{Ar}$  sanidine ages for the  
 421 Huckleberry Ridge Tuff, Yellowstone, USA: *Geology*, v. 42, no. 8, p. 643-646.

422 Robock, A., Ammann, C. M., Oman, L., Shindell, D., Levis, S., and Stenchikov, G., 2009,  
 423 Did the Toba volcanic eruption of~ 74 ka BP produce widespread glaciation?: *Journal*  
 424 *of Geophysical Research: Atmospheres*, v. 114, no. D10.

425 Roche, O., Buesch, D. C., and Valentine, G. A., 2016, Slow-moving and far-travelled dense  
 426 pyroclastic flows during the Peach Spring super-eruption: *Nature communications*, v.  
 427 7, p. 10890.

428 Rose, W. I., Conway, F. M., Pullinger, C. R., Deino, A., and McIntosh, W. C., 1999, An  
 429 improved age framework for late Quaternary silicic eruptions in northern Central  
 430 America: *Bulletin of Volcanology*, v. 61, no. 1-2, p. 106-120.

431 Rougier, J., Sparks, R. S. J., Cashman, K. V., and Brown, S. K., 2018, The global magnitude–  
 432 frequency relationship for large explosive volcanic eruptions: *Earth and Planetary*  
 433 *Science Letters*, v. 482, p. 621-629.

434 Sawi, T. M., and Manga, M., 2018, Revisiting short-term earthquake triggered volcanism:  
 435 *Bulletin of Volcanology*, v. 80, no. 7, p. 1-9.

436 Self, S., 2015, Explosive super-eruptions and potential global impacts, *Volcanic Hazards,*  
 437 *Risks and Disasters*, Elsevier, p. 399-418.

438 Seropian, G., Kennedy, B. M., Walter, T. R., Ichihara, M., and Jolly, A. D., 2021, A review  
 439 framework of how earthquakes trigger volcanic eruptions: *Nature Communications*, v.  
 440 12, no. 1, p. 1-13.

441 Shishkin, N., 2007, Seismic efficiency of a contact explosion and a high-velocity impact:  
 442 *Journal of Applied Mechanics and Technical Physics*, v. 48, no. 2, p. 145-152.

443 Storey, M., Roberts, R. G., and Saidin, M., 2012, Astronomically calibrated 40Ar/39Ar age  
 444 for the Toba supereruption and global synchronization of late Quaternary records:  
 445 *Proceedings of the National Academy of Sciences*, v. 109, no. 46, p. 18684-18688.

446 Sumita, I., and Manga, M., 2008, Suspension rheology under oscillatory shear and its  
 447 geophysical implications: *Earth and Planetary Science Letters*, v. 269, no. 3-4, p. 468-  
 448 477.

449 Svensson, A., Bigler, M., Blunier, T., Clausen, H. B., Dahl-Jensen, D., Fischer, H., Fujita, S.,  
 450 Goto-Azuma, K., Johnsen, S., and Kawamura, K., 2013, Direct linking of Greenland  
 451 and Antarctic ice cores at the Toba eruption (74 ka BP): *Climate of the Past*, v. 9, no.  
 452 2, p. 749-766.

453 Toohey, M., Krüger, K., Sigl, M., Stordal, F., and Svensen, H., 2016, Climatic and societal  
 454 impacts of a volcanic double event at the dawn of the Middle Ages: *Climatic Change*,  
 455 v. 136, no. 3, p. 401-412.

456 Wang, T., Schofield, M., Bebbington, M., and Kiyosugi, K., 2020, Bayesian modelling of  
 457 marked point processes with incomplete records: volcanic eruptions: *Journal of the*  
 458 *Royal Statistical Society: Series C (Applied Statistics)*, v. 69, no. 1, p. 109-130.

459 Watts, A. W., Greeley, R., and Melosh, H., 1991, The formation of terrains antipodal to major  
 460 impacts: *Icarus*, v. 93, no. 1, p. 159-168.

461 Williams, M., 2012, The ~ 73 ka Toba super-eruption and its impact: history of a debate:  
 462 *Quaternary International*, v. 258, p. 19-29.

463  
 464 **Acknowledgments**

465 **Funding:** ACDL acknowledges funding support from the Deutsche Forschungsgemeinschaft  
 466 (DFG) grants SCHM 2521/6-1 and KU2685/7-1; TM acknowledges funding support from the  
 467 Crosby Postdoc Fellowship at MIT; SdeS acknowledges support from National Science  
 468 Foundation grant EAR 1551187 for studies of the Toba caldera. **Author contributions:**  
 469 Conceptualization ACdeL, TM, SdeS, SS, AKS, SK; Methodology: TM, ACdeL; Formal  
 470 analysis: TM; Investigation: ACdeL, TM; Visualization: ACdeL, TM; Writing – original draft:  
 471 ACdeL, TM; Writing – review & editing: ACdeL, TM, SdeS, SS, AKS, SK. **Competing**  
 472 **interests:** The authors declare no competing interests. **Data and materials availability:** All

473 data used in this study are from previously published work, no new data was collected as part  
474 of this study. In the final manuscript, we will provide the Python notebook for analysis as  
475 supplementary material.

476